



*Research article*

## **Mass Spectrometry Imaging of Chlorhexidine and Bacteria in a Model Wound**

**Timothy Hamerly<sup>1</sup>, Margaret H. Butler<sup>2</sup>, Steve T. Fisher<sup>3</sup>, Jonathan K. Hilmer<sup>1</sup>, Garth A. James<sup>3</sup>, and Brian Bothner<sup>1\*</sup>**

1 Department of Chemistry and Biochemistry, Montana State University, Bozeman MT 59717, USA

2 BioScience Laboratories Inc., Bozeman MT 59718, USA

3 Center for Biofilm Engineering, Montana State University, Bozeman MT 59717, USA

\* **Correspondence:** Email: [bbothner@chemistry.montana.edu](mailto:bbothner@chemistry.montana.edu); Tel: (406)-994-5270;  
Fax: (406)-994 5407

**Abstract:** The ability to generate two-dimensional images of a wound that contains information about the distribution of bacteria overlaid with the distribution of drugs and metabolites could enhance our understanding of wound healing processes. Advances in technology are leading to a rapid expansion in mass spectrometry-based imaging. When combined with the ability of matrix assisted laser desorption ionization to ionize a wide range of molecules, imaging mass spectrometry is a powerful biomedical research tool. However, this technique has yet to be used to investigate bacterial colonization of wounds or the distribution of antimicrobial agents on tissue. To address this, distribution and persistence of the antimicrobial agent chlorhexidine on a model human tissue was investigated. The ability to detect and localize *Staphylococcus aureus* on the same tissue model was also addressed. Sub-millimeter resolution ion images from these experiments show the promise of using mass spectrometry imaging to investigate the growth and treatment of bacteria on skin. This methodology will be of value in the development of wound dressings with improved antimicrobial properties and a more careful analysis of the concentration of antimicrobial agents required to prevent biofilm formation and persistence.

**Keywords:** chlorhexidine; chronic wound; MALDI-IMS; mass spectrometry imaging

---

## 1. Introduction

Acute and chronic wounds are a major healthcare concern. Millions of Americans are affected each year and it is estimated that associated costs are greater than 25 billion dollars annually [1–3]. A wound is defined as the disruption of normal anatomic structure and function of a tissue or organ [2,4]. Wounds can be classified into two categories, acute and chronic. Acute wounds progress through a sequential process of healing, resulting in the restoration of anatomic and functional integrity [4]. Chronic wounds are those which fail to heal in an orderly and timely fashion, leaving anatomical and functional integrity unrestored [4]. Chronic wounds often result in hospital stays, costing patients both time and money [1–4]. Additionally, there is an increased risk for patients with chronic wounds to develop infections, lengthening the time to heal and further increasing cost of treatment [3,4]. Bacterial infections can be present in both types of wounds and can further complicate the healing process, particularly if biofilms develop. Often, chronic wounds are a direct result of biofilm infections, where normal healing processes become disrupted due to the presence of bacteria in the biofilm [2]. Antimicrobial agents for the treatment of infected wounds have been developed by major healthcare corporations and include ionic/elemental silver, povidone-iodine, and chlorhexidine gluconate (CHG) [2].

CHG came from synthetic efforts in the mid 1950's to find new compounds which exhibited antimicrobial activity [5]. Along with other bisdiguanydes, it has strong antibacterial activity and is used for wound dressings, oral care, and pre/post-operative showering or bathing [5–11]. CHG is a cationic bisbiguanide with broad antimicrobial activity, low mammalian toxicity, and a strong affinity for binding to skin and mucous membranes [12–14]. At low concentrations, CHG is bacteriostatic and at higher concentrations is an effective bactericide, active against both gram-positive and gram-negative bacteria [12,14,15]. Due to its positive charge at physiological pH, CHG binds tightly to negatively charged membranes and cell walls of bacteria, where it disrupts integrity of the barrier, leading to the release of potassium ions, phosphorus ions, and pentose sugars, as well as inhibiting ATPase activity [13–15]. At higher concentrations, CHG causes the cytoplasm contents to precipitate, leading to cell death [13–15]. The effectiveness of CHG has made it a leading antimicrobial agent for coating wound dressings as a deterrent to infection [16,17].

Despite nearly 60 years of general use as a wound care agent and an extensive body of literature supporting the use of CHG on wound dressings, studies to investigate localization and persistence within wounds are limited. In part, this is due to the difficulty associated with collecting analytical data with high spatial resolution. The advent of mass spectrometry-based imaging now makes it possible to collect data on the presence of molecules across a wide-range of molecular weights [18–20]. One of the leading technologies in this area is matrix assisted laser desorption ionization imaging mass spectrometry (MALDI-IMS). In this technique, a matrix is applied to sectioned tissue. When exposed to a focused UV laser, analytes (e.g. CHG) become ionized and subsequently mass is measured using a time of flight (TOF) mass spectrometer [19]. By rastering the laser across the tissue and measuring the abundance of ions at each spot (pixel), a two-dimensional image based on ion intensity can be generated. A schematic of the general MALDI-IMS method as used in this study is shown in Figure 1. By stacking images, a full spatial representation of a wound in three-dimensions can be created. To investigate the interaction of CHG and wounded skin, *in vitro* tissue samples with artificial wounds produced by a biopsy punch were treated with CHG to mimic exposure from a dressing, and analyzed using MALDI-IMS. In addition to investigating the

localization and penetration of CHG on in vitro tissue samples, tissue contaminated with *Staphylococcus aureus* was also analyzed. This study demonstrates that MALDI-IMS can be used to track the distribution of bacteria and antimicrobial agents on wounded tissue.

## 2. Materials and Method

### 2.1. Reagents

All solvents for MALDI analysis were of HPLC grade; water from Avantor (Center Valley, PA) and methanol from EMD Chemicals Inc. (Gibbstown, NJ). Gelatin for cyrosectioning was purchased from Hardy Diagnostics (Cat. No. C7921, Santa Maria, CA). The matrix 2,5-dihydroxybenzoic acid (DHB) was purchased from Alfa Aesar (Cat. No. A11459, Ward Hill, MA) and formic acid (98% GR ACS) for use as an ion pairing agent was purchased from EMD Chemicals Inc. (Gibbstown, NJ). CHG digluconate (CHG) 20% w/v in H<sub>2</sub>O for serial dilutions was purchased from Sigma-Aldrich (CAS No. 018472-51-0, St. Louis, MO). Indium tin oxide (ITO) coated glass slides for MALDI-IMS were purchased from Bruker Daltoniks GmbH (Cat. No. 237001, Bremen, Germany). Tryptic soy broth (TSB, Soybean-Casein Digest Medium) for growth of *Staphylococcus aureus* 10943 was purchased from BD Diagnostics (Cat. No. 211825, Franklin Lakes, New Jersey). EpiDermFT (EFT-300) tissue samples were obtained from MatTek Corporation (Ashland, MA) with a 3 mm wound generated by biopsy punch. Physiological saline (0.9%) was obtained from Hospira, Inc. (Lake Forest, Illinois).

### 2.2. Sectioning of tissue samples

Tissue samples were sectioned as previously described by Ye *et al.* [22]. Briefly, tissues were embedded in 100 mg/mL gelatin, and flash frozen in an ethanol/dry ice bath. Frozen tissues were stored at -80 °C until sectioning. For sectioning, 5 µm slices were produced with a cryostat at -20 °C, and thaw mounted directly onto ITO glass slides. Following sectioning, tissue slices were dehydrated in a desiccator before being coated with DHB matrix (150 mg/mL in 50% aqueous methanol with 0.05% formic acid) using an airbrush. Airbrush application was done using a paint airbrush sprayer, held approximately 25 cm from the slide, moving in a zig-zag pattern for approximately 30 seconds, followed by 1 minute drying time. This was repeated until 15 mL of matrix solution had been dispensed (approximately 10 passes). Matrix coated samples were placed in a desiccator to dehydrate until analysis by MALDI-IMS.

### 2.3. Growth of *S. aureus* and placement on sectioned tissue

*Staphylococcus aureus* strain 10943 was used in this study and is a methicillin-resistant clinical wound isolate obtained from the Southwest Regional Wound Care Center (Lubbock, TX) that has been previously used for biofilm evaluation of antimicrobial wound dressings [23,24]. To prepare the bacteria, a tube of tryptic soy broth (10 mL) was inoculated from a frozen stock culture and incubated at 37 °C overnight to achieve an approximate cell density of 10<sup>8</sup> CFU/mL. Ten-fold serial dilutions were then prepared in phosphate-buffered saline to achieve the desired bacterial concentrations. Actual bacterial concentrations were determined by plate count on tryptic soy agar.

Bacteria at four concentrations ( $10^8$ ,  $10^7$ ,  $10^6$ , and  $10^5$  CFU/mL) were placed on top of sectioned tissue using a pipet before being coated with DHB matrix for MALDI-IMS analysis.

#### 2.4. MALDI-MS data acquisition for calibration curve of CHG standard and analysis

Data was collected using a Bruker autoflex III MALDI-TOF/TOF mass spectrometer (Bruker Daltonics, Billerica, MA) equipped with a Smartbeam Nd:YAG 355 nm laser. The instrument was operated in positive ion mode using the TOF reflectron. Bruker flexControl v3.3 software was used to control the instrument and data analysis was done using flexAnalysis v3.3 (Bruker Daltonics, Billerica, MA). A 20% CHG (w/v) in water stock solution was diluted in HPLC grade water; 1:1000 (0.02% w/v), 1:2000 (0.01% w/v), 1:5000 (0.004% w/v), 1:10,000 (0.002% w/v), 1:20,000 (0.001% w/v), 1:50,000 (0.0004% w/v), and 1:100,000 (0.0002% w/v) for the standard curve. Spots were placed onto a Bruker MTP 384 Polished Steel TF target plate (Part No. 8209520) for analysis.

#### 2.5. MALDI-IMS data acquisition and analysis for CHG and staph on tissue samples

Image data was collected using an automated method with the following settings. Spectra from tissue samples were generated by averaging 500 laser shots for each pixel. The sample was rastered at a resolution of  $200 \times 200 \mu\text{m}$ . Data files were analyzed using fleximaging v2.1 software (Bruker Daltonics, Billerica, MA) or exported as an IMG file (.img) and imported into MSiReader v0.05 (North Carolina State University). For each experiment data was normalized by total ion count using the flexImaging software, relative to the noise level, in order to facilitate direct comparisons across each image generated.

### 3. Results

#### 3.1. Generation of CHG standard curve

To assess the potential for using MALDI-IMS as a quantitative tool for the analysis of CHG, the first step was to demonstrate that CHG could be detected at relevant levels and that a reproducible standard curve could be generated. A dilution series of CHG was spotted onto the analysis plate and analyzed using 2,5-dihydroxybenzoic acid (DHB) matrix. The mass spectrum obtained from each dilution showed intense ions at 505.2 and 507.2 m/z which match the expected CHG isotope pattern due to the presence of chlorine,  $^{35}\text{Cl}$  and  $^{37}\text{Cl}$  respectively (Figure 2A). A change in signal intensity for the isotope distribution was observed for the different samples. Using this data, a standard curve was generated from a dilutions series in which CHG stock solution (20% w/v in  $\text{H}_2\text{O}$ ) was diluted in water to final concentrations of 0.02% w/v to 0.0002% w/v. The standard curve was based on intensity of the monoisotopic peak of CHG (molecular weight of 504.2 [M+H equals 505.2] and chemical formula of  $\text{C}_{22}\text{H}_{30}\text{Cl}_2\text{N}_{10}$ ). The coefficient of determination was 0.98 across two orders of magnitude for the dilution series (Figure 2B).

#### 3.2. Detection and localization of CHG on tissue assessed by MALDI-IMS

Having ascertained that CHG could be measured at clinically relevant concentrations, we next

moved to the analysis of sectioned tissue samples treated with CHG. In vitro tissue samples which had a wound induced via biopsy punch were gently washed with a solution of 0.05% (w/v) CHG. Following this, tissue samples were flash frozen in a gelatin matrix and subsequently sectioned in 5  $\mu\text{m}$  slices onto indium-tin-oxide (ITO) coated glass slides. Slides were then sprayed with DHB before MALDI-IMS analysis (Figure 1). Each tissue section is surrounded by a gelatin matrix to aid sectioning. The induced wound was located on the left side after sectioning (Figure 3B–D) and was the surface of the tissue to which CHG was applied prior to sectioning. Each pixel in the image was generated by summing 500 laser shots. The three images are sequential sections from the same tissue sample analyzed in one imaging sequence. Data was acquired in  $200 \times 200 \mu\text{m}$  steps, moving from left to right, top to bottom. The ion intensity of CHG was extracted from each pixel and converted into an ion density map for each tissue section (Figure 3B–D). CHG abundance was localized to the wound site.

### 3.3. Imaging of *Staphylococcus aureus* in wounds

Having shown that MALDI-IMS can be used in a targeted approach to detect CHG on tissue, the next step was to see if bacteria could be detected on tissue. *S. aureus* is a gram positive bacterium found on the skin. It is a common cause of skin and wound infections. To investigate the potential for using MALDI-IMS for the detection of *S. aureus*, the same experimental method used for CHG imaging was repeated. Sectioned tissue was spotted with *S. aureus* at four different concentrations. Additionally, bacterial cells were spotted directly onto the glass slide as a positive control. The slide was sprayed with DHB matrix and analyzed using MALDI-IMS. Figure 4A shows a diagram of the layout of tissue and cells placed on an ITO coated MALDI slide. Decreasing numbers of *S. aureus* were spotted in the center of each tissue section.

Unlike the CHG experiment, the molecular signature for *S. aureus* was not known. Therefore the entire data range (100 to 1000  $m/z$ ) needed to be analyzed for ions that could be used for creating an image. Ions uniquely associated with the bacteria and the tissue were mined using MSiReader software. MSiReader allows a user to select an area of interest and compare it to a reference area, pulling out features unique to the area of interest above a signal-to-noise (S/N) threshold of 10. A series of eight ions unique to *S. aureus* were found by analyzing an area containing only bacterial cells (Table 1). A second set of 10 ions unique to tissue were also identified. Features from these lists were used to map bacterial cells and tissue. Using the ions 229.4 and 260.5  $m/z$ , images were generated to map *S. aureus* and tissue respectively (Figure 4B and C). These two ions were selected to generate images due to the fact that their average intensity is in the middle of those measured in Table 1, thus giving a good representation of overall image quality. Overlaying the two data sets produced a complete image of the tissue surface which revealed the precise location of *S. aureus* (Figure 4D). In the overlay heat map image blue represents *S. aureus* and red represents tissue. As can be seen in panels 4C and 4D, the ions specific for *S. aureus* are only seen when lower cell concentrations are spotted onto the slide ( $10^6$  and  $10^5$  cells respectively). Suppression of ionization can occur under certain sample conditions, particularly when analytes are at high concentrations, such as was the case when high cell concentrations were used [25,26]. Using MALDI-IMS, molecular features can be used to distinguish tissue from cells in a spatially resolved environment.

**Table 1. Ions unique to specific samples.**

<b>S. aureus</b>		<b>Tissue</b>	
<b>m/z</b>	<b>Intensity</b>	<b>m/z</b>	<b>Intensity</b>
142.7	28	103.9	250
192.6	46	109.2	21
198.6	434	109.8	22
213.5	54	114.9	79
229.4	26	153.8	41
360.1	33	183.7	238
376.0	21	238.6	46
391.9	22	260.5	72
		272.4	145
		282.4	59

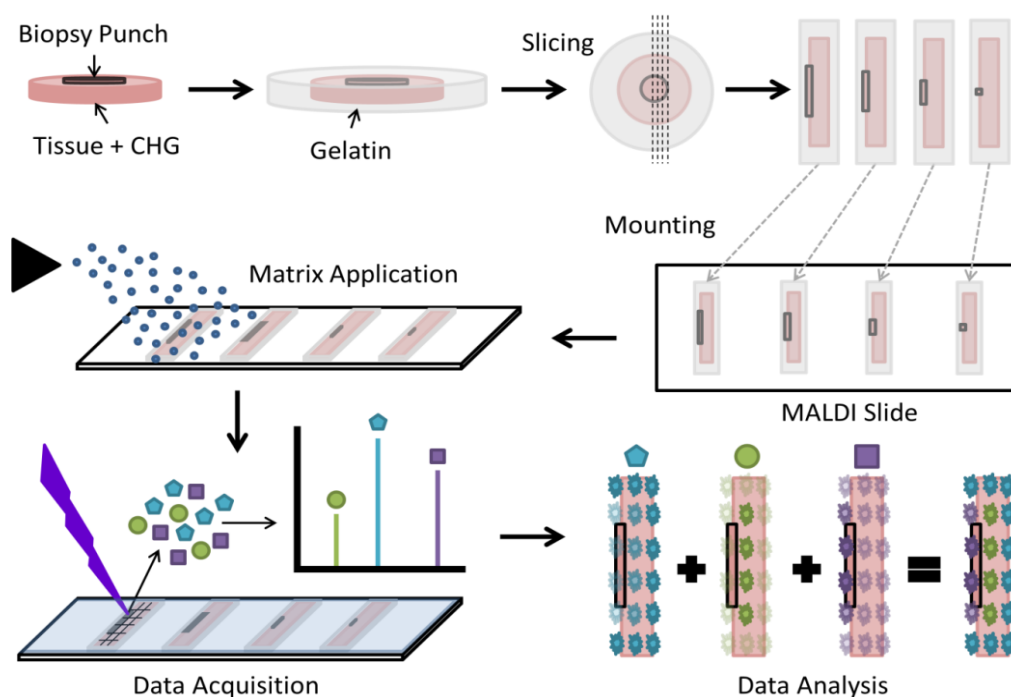


**Figure 1. Diagram depicting the method for analyzing tissue samples using matrix assisted laser desorption/ionization—imaging mass spectrometry (MALDI-IMS).** Tissue samples which have been treated with CHG and have a bacteria on them are coated in gelatin for cyrosectioning. Sections are placed onto special MALDI microscope slides coated with indium-titanium oxide. The slide is then coated in matrix for MALDI analysis and after drying, slides with tissues are placed in the MALDI-MS. The laser then rasters the entire tissue section, generating a spectrum each time. These spectra are then analyzed to generate an image of ions where intensity of a color indicated how much of that particular ion is seen at any given spot on the tissue.

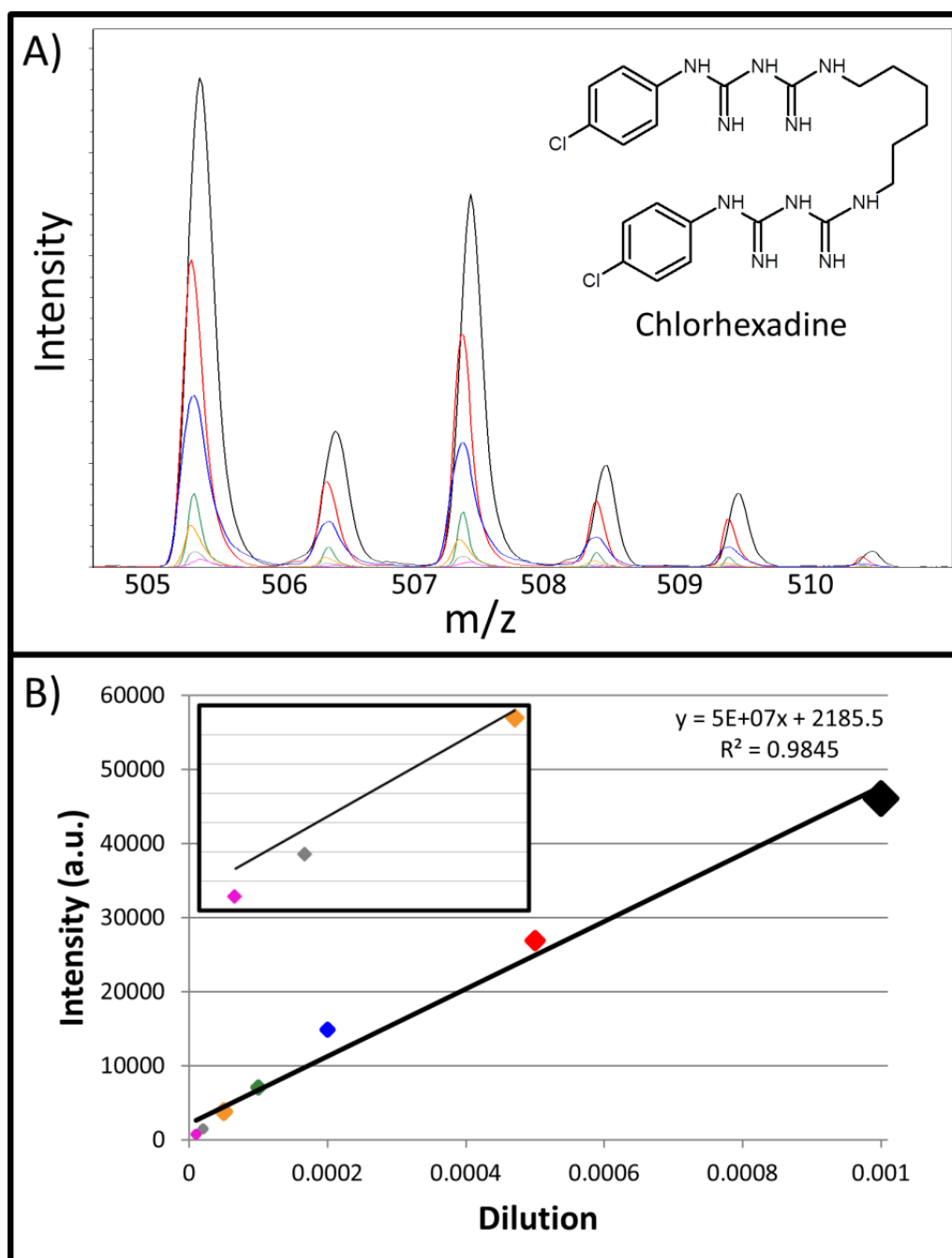


**Figure 2. Standard curve for chlorhexidine generated using MALDI-MS. Close up of mass spectra for CHG at seven different concentrations.** The peaks at 505.2 and 507.2 correspond to the two common isotopes of chlorine ( $^{35}\text{Cl}$  and  $^{37}\text{Cl}$ ), where 505.2 represents the monoisotopic mass. Using this data, a standard curve for measuring CHG was generated, panel B. The ion intensity data was linear across two orders of magnitude for chlorhexidine (CHG) concentration. The size of the diamond represents the error associated with the data point, where  $n = 3$  and 500 laser shots were summed per  $n$ . The inset in Panel B shows a zoom of the three lowest dilutions, where the size of the diamond again represent the error. Spectrum and line colors are consistent between panels. The structure of CHG is shown in Panel A.

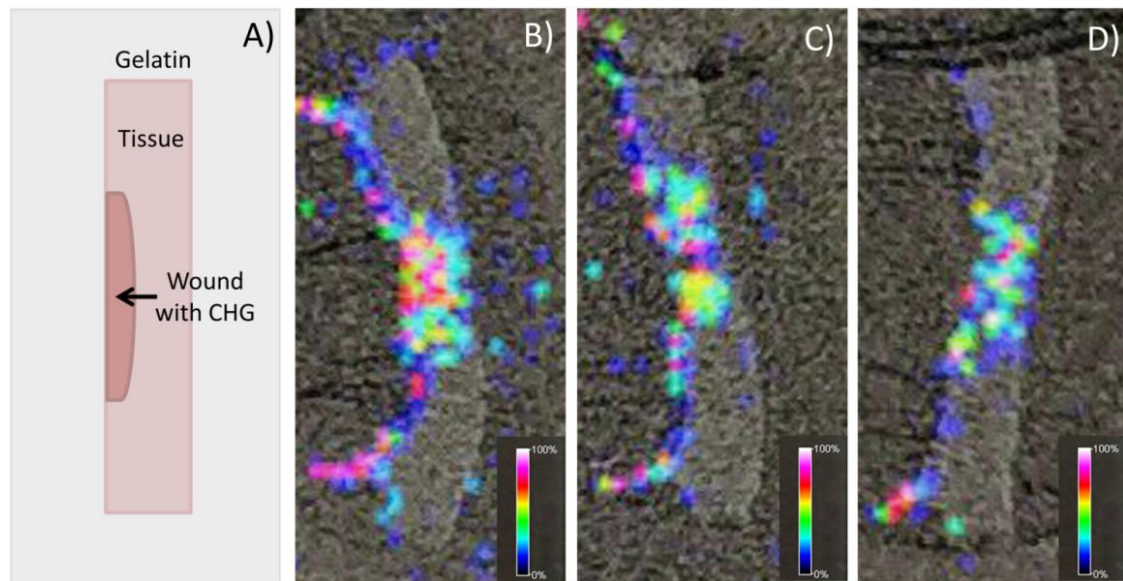


**Figure 3. Images showing CHG concentration across a section of wounded tissue. Panel A shows a schematic diagram of each tissue on a slide.** Tissue sections are surrounded by gelatin, and in the center of the tissue is a wound which has been treated with CHG. CHG was placed only on the top of the tissue, which in these figures is the left hand side of the tissue section. Panels B, C, and D show sections moving from the center to the periphery of the wound, respectively. The color scale at the bottom right of each image shows the intensity of CHG (blue = low, white = high). A decrease in CHG signal was observed moving from the center outward ( $B > C > D$ ).



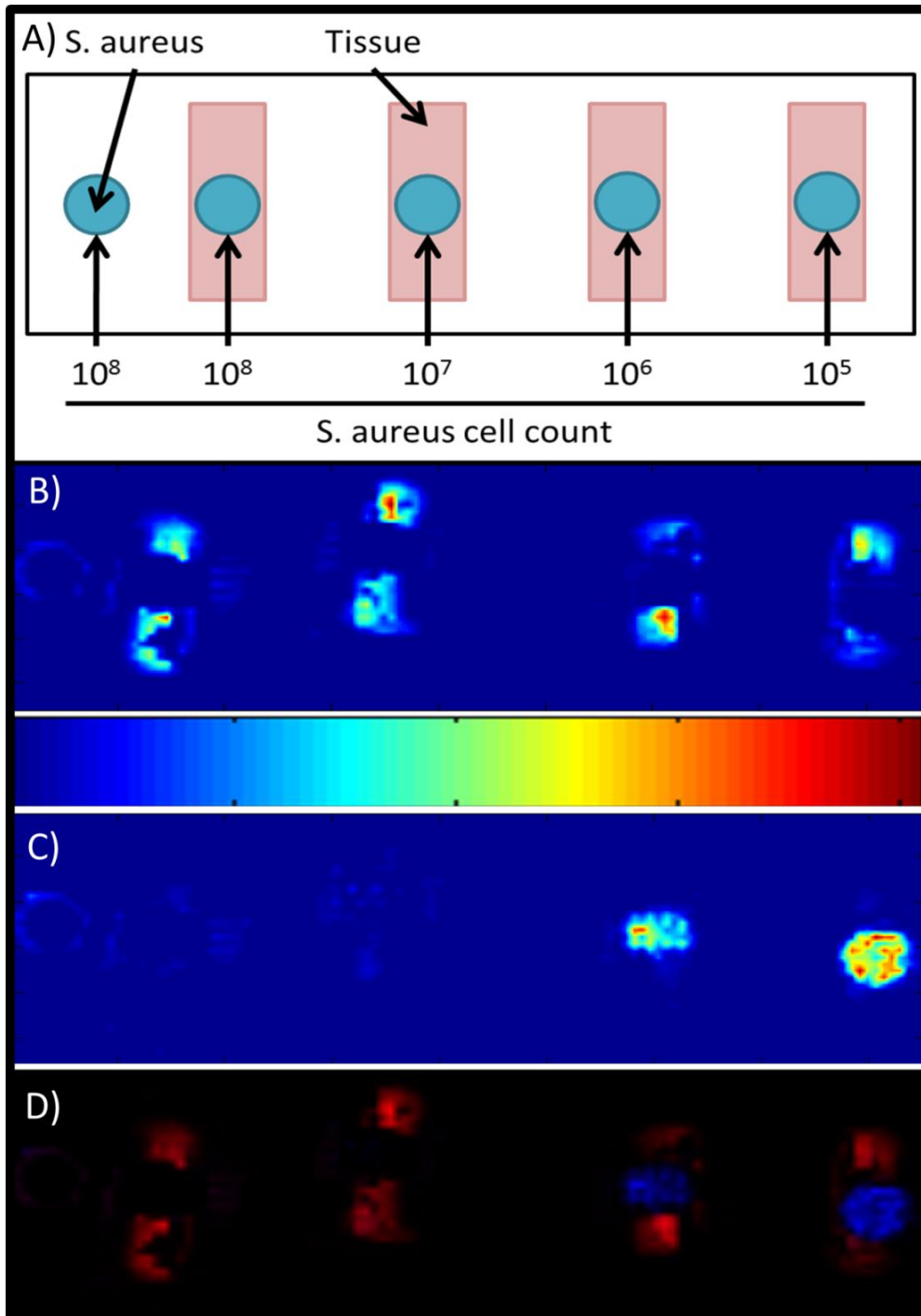


**Figure 4. Imaging of *S. aureus* on tissue. Panel A is a diagram depicting the layout for the MALDI-IMS data shown below. From left to right; A spot of  $10^8$  cells was placed directly on the glass tissue as a reference to aid in finding unique features to the bacteria. Panels B and C use a unique feature for identifying tissue (B) and cells (C) which corresponds to  $m/z$  of 260.5 and 229.4 respectively. The scale to the right shows relative ion intensity. Scale is from blue (low) to red (high). Panel D shows the overlay of B and C. The red color indicates the feature (260.5) unique to tissue samples, while the blue color represents the feature (229.4) unique to *S. aureus*.**

#### 4. Discussion

The ability to detect CHG across a wide range of concentrations demonstrates that MALDI-MS analysis of the antimicrobial agent has the potential to quantify the amount in a sample of interest. The characteristic pattern of isotope peaks due to the chlorine isotopes ( $^{35}\text{Cl}$  and  $^{37}\text{Cl}$ ) makes CHG easy to identify in the spectrum, as there are few molecules which would be present in a biological sample that contain chlorine ions. With the knowledge that CHG can be detected and quantified, analysis of *in vitro* tissue samples after injury was attempted (Figure 3). Results from these experiments show that CHG ion intensity was concentrated in the region where the biopsy punch was made. No CHG was found to be present on control samples which did not receive biopsy punch prior to CHG treated as expected (data not shown). The highest observed intensity was in the tissue section taken from the center of the wound (Figure 3B), moving outward from the center of the wound (Figure 3C and D) signal intensity decreased, suggesting that CHG is retained better by damaged tissue. A relatively low concentration of CHG was observed on the left side of the tissue section. This surface was the top of the tissue before sectioning and the residual is likely due to weakly bound CHG remaining on the surface after washing and is to be expected as CHG is known to bind the surface of tissues [12–14]. No penetration into the tissue can be seen outside the area of the wound. This is consistent with the idea that CHG does not penetrate the outer most layer of epidermis, except where there is a lesion or break in the skin. Additionally, it does not appear that CHG diffuses away from the site of the wound. The ability to image CHG in a semi-quantitative manner shows the potential for MALDI-IMS as a tool for studying the distribution, penetration, and persistence of CHG directly from tissue and wounds.

Following the analysis of CHG on tissue samples, MALDI-IMS was applied to tissue samples which were sectioned and spotted with *S. aureus*. The goal of this analysis was to determine if chemically unique features for tissue and bacterial cells could be used to generate an image. Our results show that this is feasible. The images shown in Figure 4 clearly delineate the location of *S. aureus*. The images were produced based on the distribution of two ions (260.5 and 229.4). MALDI-IMS data is very rich, suggesting that complex images displaying numerous chemical distributions can be generated. Interestingly, the unique molecular features for the bacterial cells were only present with the lower concentration of cells. When greater numbers of *S. aureus* were present, an overall ion suppression in those pixels was observed. A likely explanation is that at very high cell concentration suppression of the MALDI process is occurring [25,26]. This may be an artifact of the experimental method used here, however, further testing would need to be conducted. These results demonstrate that bacteria can be imaged on tissue using MALDI-IMS and suggest that this method could be used to investigate growth on tissue and wound models.

Using standard MALDI-IMS methodology, images with sub-millimeter resolution can be produced. Unique chemical signals can be used to localize bacteria and antimicrobial agents. The distribution of the antimicrobial compound CHG was determined for tissue sections from an *in vitro* wound model system. The results show that CHG remains localized to the area around the wound and that penetration into the tissue at the wound site was minimal. The common skin bacteria and clinically relevant infectious agent *S. aureus* produced eight unique ions. Together, these results suggest that MALDI-IMS can be a powerful tool for studying bacterial colonization of wounds and how the distribution of compounds such as CHG in and around wounds impacts bacteria. The relatively high spatial resolution and specific mass signals of MALDI-IMS offers distinct advantages

over other techniques. Future studies will be needed to assess if the technique works for other bacterial strains and other antimicrobial agents. Also, more detailed level of detection and level of quantification studies will be needed to establish how broadly applicable the method will be.

## Acknowledgments

Tim Hamerly would like to recognize support from the Kopriva Graduate Fellowship at MSU. The mass spectrometry facility at MSU receives funding from the Murdock Charitable Trust and NIH 5P20RR02437 of the CoBRE program. We would like to acknowledge Jesse Thomas for technical assistance with MALDI-TOF instrumentation. The authors would like to thank Erin Gemperline for her advice on cyrosectioning, matrix application techniques, data acquisition and analysis.

## Conflict of Interest

The authors claim no conflict of interest.

## References

1. James GA, Swogger E, Wolcott R, et al. (2007) Biofilms in chronic wounds. *Wound Repair Regen* 16: 37–44.
2. Brackman G, De Meyer L, Nelis HJ, et al. (2013) Biofilm inhibitory and eradicating activity of wound care products against *Staphylococcus aureus* and *Staphylococcus epidermidis* biofilms in an in vitro chronic wound model. *J Appl Microbiol* 114: 1833–1842.
3. Demidova-Rice TN, Hamblin MR, Herman IM (2012) Acute and impaired wound healing: pathophysiology and current methods for drug delivery, part 1: normal and chronic wounds: biology, causes, and approaches to care. *Adv Skin Wound Care* 25: 304–314.
4. Lazarus GS, Cooper DM, Knighton DR, et al. (1994) Definitions and guidelines for assessment of wounds and evaluation of healing. *Wound Repair Regen* 2: 165–170.
5. Davies G, Francist J, Martin A, et al. (1954) 1:6-Di-4'-Chlorophenyldiguanidohexane ("Hibitane"\*). Laboratory investigation of a new antibacterial agent of high potency. *Brit J Pharm Chemoth* 9: 192–196.
6. Ayliffe GAJ, Noy MF, Babb JR, et al. (1983) A comparison of pre-operative bathing with soap in the prevention of wound infection. *J Hosp Infect* 4: 237–244.
7. Hayek LJ, Emerson JM, Gardner AMN (1987) A placebo-controlled trial of the effect of two preoperative baths or showers with chlorhexidine detergent on postoperative wound infection rates. *J Hosp Infect* 10: 165–172.
8. Garibaldi RA (1988) Prevention with of intraoperative chlorhexidine wound contamination shower and scrub. *J Hosp Infect* 11: 5–9.
9. Lynch W, Davey PG, Malek M, et al. (1992) Cost-effectiveness analysis of the use of chlorhexidine detergent in preoperative whole-body disinfection in wound infection prophylaxis. *J Hosp Infect* 21: 179–191.
10. Jeansonne MJ, White RR (1994) A Comparison of 2.0% chlorhexidine gluconate and 5.25% sodium hypochlorite as antimicrobial endodontic irrigants. *J Endodont* 20: 276–278.

11. McBain AJ, Bartolo RG, Catrenich CE, et al. (2003) Effects of a chlorhexidine gluconate-containing mouthwash on the vitality and antimicrobial susceptibility of in vitro oral bacterial ecosystems. *Appl Environ Microb* 69: 4770–4776.
12. Jones CG (1997) Chlorhexidine: is it still the gold standard? *Periodontol* 2000 15: 55–62.
13. Zong Z, Kirsch LE (2012) Studies on the instability of chlorhexidine, Part I: kinetics. *J Pharm Sci* 101: 2417–2427.
14. Hidalgo E, Dominguez C (2001) Mechanisms underlying chlorhexidine-induced cytotoxicity. *Toxicol in Vitro* 15: 271–276.
15. Russell AD (1986) Chlorhexidine: antibacterial action and bacterial resistance. *Infection* 14: 212–215.
16. Agarwal A, Nelson TB, Kierski PR, et al. (2012) Polymeric multilayers that localize the release of chlorhexidine from biologic wound dressings. *Biomaterials* 33: 6783–6792.
17. Lavoine N, Tabary N, Desloges I, et al. (2014) Controlled release of chlorhexidine digluconate using  $\beta$ -cyclodextrin and microfibrillated cellulose. *Colloids Surfaces B* 121: 196–205.
18. Caprioli RM, Farmer TB, Gile J (1997) Molecular imaging of biological samples: Localization of peptides and proteins using MALDI-TOF MS. *Anal Chem* 69: 4751–1760.
19. Chughtai K, Heeren RMA (2010) Mass spectrometric imaging for biomedical tissue analysis. *Chem Rev* 110: 3237–3277.
20. Hart PJ, Francese S, Claude E, et al. (2011) MALDI-MS imaging of lipids in ex vivo human skin. *Anal Bioanal Chem* 401: 115–125.
21. Kaluzhny Y, Kandárová H, Hayden P, et al. (2011) Development of the EpiOcular™ eye irritation test for Hazard identification and labelling of eye irritating chemicals in response to the requirements of the EU. *Altern Lab Anim* 39: 339–364.
22. Ye H, Gemperline E, Venkateshwaran M, et al. (2013) MALDI mass spectrometry-assisted molecular imaging of metabolites during nitrogen fixation in the *Medicago truncatula*-*Sinorhizobium meliloti* symbiosis. *Plant J* 75: 130–145.
23. Ammons MCB, Ward LS, James GA (2011) Anti-biofilm efficacy of a lactoferrin/xylitol wound hydrogel used in combination with silver wound dressings. *Int Wound J* 8: 268–273.
24. Agostinho AM, Hartman A, Lipp C, et al. (2011) An in vitro model for the growth and analysis of chronic wound MRSA biofilms. *J Appl Microbiol* 111: 1275–1282.
25. Knochenmuss R, Zenobi R (2003) MALDI ionization: The role of in-plume processes. *Chem Rev* 103: 441–452.
26. Annesley T M (2003) Ion suppression in mass spectrometry. *Clin Chem* 49: 1041–1044.



AIMS Press

© 2015 Brian Bothner et al., licensee AIMS Press. This is an open access article distributed under the terms of the Creative Commons Attribution License (<http://creativecommons.org/licenses/by/4.0>)